Buried stressors in nitride semiconductors: Influence on electronic properties

A. E. Romanov,[a] P. Waltereit, and J. S. Speck
Materials Department, University of California, Santa Barbara, California 93106

(Received 30 March 2004; accepted 28 November 2004; published online 26 January 2005)

An analysis is presented on the effect of the strain field originating from a subsurface stressor (point source of dilatation or a dilatating ellipsoidal inclusion) on the electronic properties of nitride semiconductors. With good accuracy, real quantum dots can be modeled as such stressors. We consider the following material structure design: a uniform semi-infinite GaN matrix with a buried stressor or a GaN matrix with a single (In,Ga)N quantum well, which is grown pseudomorphically between the stressor and the free surface. We utilize isotropic elasticity to determine the strain field in the structures under investigation. We then apply a $\mathbf{k}\cdot\mathbf{p}$ perturbation theory approach to examine the shifts of the conduction and valence band edges caused by the stressor. We find lateral confinement for electrons and holes, which can be proposed for the realization of strain-induced quantum dots in the quantum well. © *2005 American Institute of Physics*.
[DOI: 10.1063/1.1851016]

I. INTRODUCTION

The distinguishing properties of nitride semiconductors include their large spontaneous polarization and large piezoelectric coefficients. In nitride-based heterostructures, discontinuities in spontaneous polarization coupled with piezoelectric generated polarization caused by lattice mismatch give rise to large internal electric fields. In addition, the effect of elastic strains is magnified by large values of the deformation potentials in nitride semiconductors. A brief comparison of GaAs and GaN parameters responsible for strain-related effects is given in Table I.

In general, strain-induced phenomena have a large impact on electronic properties of semiconductors[1,2] The conduction and valence band levels and the band gap can be modified by strain. Strain-induced piezoelectric polarization charges lead to electrostatic fields of a magnitude (MV/cm) that cannot be neglected in nitride semiconductors. In fact, strain and polarization effects may be exploited to tailor heterostructures. Examples include two-dimensional electron gases at (Al,Ga)N/GaN interfaces and large internal electrostatic fields that give rise to the quantum-confined Stark effect (QCSE) in quantum wells (QWs). Such heterostructures have been studied in detail both experimentally and theoretically, the latter being facilitated by the symmetry of two-dimensional heterostructures.[3] However, little is known about the impact of deviations from the two-dimensional nature of heterostructures on device properties. These deviations may be either intentional, e.g., (In,Ga)N quantum dots (QDs),[4] and surface and subsurface stressors, or unintentional, as a result of uncontrolled thickness or composition modulation in growing multiple QWs.[5] In this article, we investigate the influence of the intentionally nonuniform strain field originating from a subsurface stressor on the electronic properties of nitride semiconductors. The stressor is chosen either as point source of dilatation or as dilatating ellipsoidal inclusion in order to account for both far- and near-field effects in tractable analytical form.

The effect of finite size of QDs (nanosized inclusions) on electronic and optoelectronic properties of semiconductor materials was intensively studied during the last decade.[6–8] The ultimate motivation for all of these studies was to describe and detect the confinement of the carriers (electrons and holes) in QDs. Originally, the confinement was attributed to the size effect on the carrier wave functions placed in three-dimensional potential boxes.[2,8] In addition, it was pointed out that due to the crystal lattice mismatch between the materials of QD and surrounding matrix, considerable elastic strains can be generated inside a QD.[9,10] Such intrinsic strains contribute to the modification of semiconductor band structure via the *deformation potentials*.[1] The influence of intrinsic strains of QDs on their electronic properties have been discussed for example in Refs. 11–13. On the other hand QDs generate nonuniform elastic strains in their vicinity modifying the physical properties of the matrix.[14] As earlier as at the end of 1980s, it was proposed to use the nonuniform strains fields originating from *surface stressors* [Fig. 1(a)] for lateral confinement of excitons and carriers[15,16] in a QW, which in turn was responsible for vertical confinement [see Fig. 1(a)]. In these reports, it was demonstrated that strain-induced lateral confinement may be achieved in InGaAs/GaAs QWs, resulting in redshifted photolumines-

TABLE I. Comparison of GaAs and GaN response to elastic strain. Data for GaAs are taken from Ref. 14; for GaN data see Sec. III.

Material	Band gap (eV)	Interband hydrostatic deformation potential (eV)	Typical magnitude for piezoelectric coefficient ($C\,m^{-2}$)
GaAs	1.42	$a_c - a_v = -7.9$	$e_{14} = -0.16$
GaN	3.45	$a_1 = \alpha_{\parallel} - D_1 = -3.1$ $a_2 = \alpha_{\perp} - D_2 = -11.2$	$e_{31} = -0.49$

[a]Permanent address: A.F. Ioffe Physico-Technical Institute, 194021 St. Petersburg, Russia; electronic mail: speck@mrl.ucsb.edu

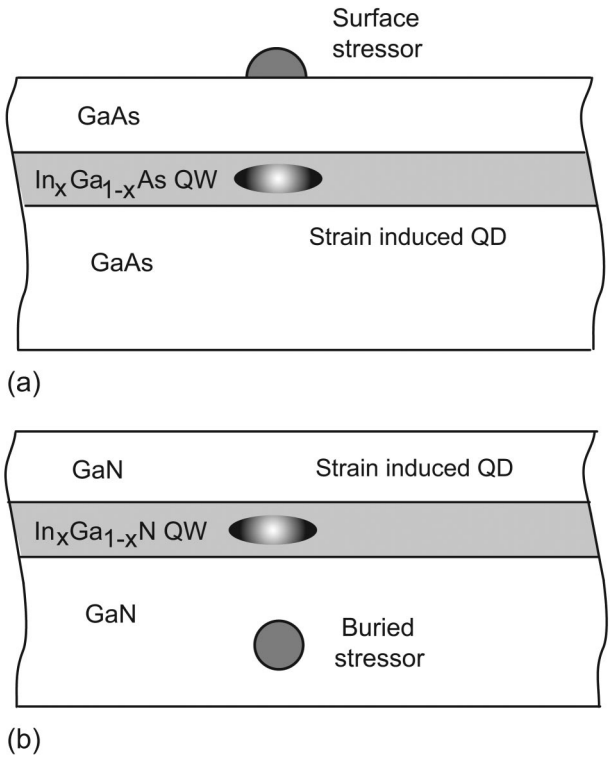

FIG. 1. Strain-induced QDs in semiconductor structures. (a) QD induced in a QW by a surface stressor, e.g., InP or InAs, in materials with zinc-blende crystal structure. (b) QD induced by buried stressor, e.g., InN, in materials with wurtzite crystal structure.

cence spectra. These and other earlier observations were summarized in Ref. 17. Later on, Tulkki *et al.*[18] examined the influence of a surface stressor on the optical properties of a buried QW and obtained good agreement with corresponding experiments by Lipsanen *et al.*[19]

Davies[20] and Schoenfeldt *et al.*[21] developed the idea that a *subsurface stressor* [Fig. 1(b)] could be used as a tool to modify the confinement in nearby QW in the case of zinc-blende structures. Davies investigated both surface[22] and subsurface[20] stressors and reported spatially direct and indirect electron-hole transitions, respectively. However, Davies neglected the presence of hydrostatic strain induced by a subsurface stressor in a semi-infinite medium. Although the properties of QDs in wurtzite semiconductors were already addressed (see, for example, the comprehensive paper by Andreev and O'Reilly[23] on the relation between the shape and size of the dot in GaN/AlN system and confined wave functions in the dot), their possible role as a subsurface stressor was not investigated. In this article, we present the development of our model for the subsurface stressors in nitride semiconductors originally proposed in Ref. 24.

An important part of the analysis of strain-induced effects relies on modeling the stressor itself, i.e., the elastic fields produced by stressor. A number of recent studies have addressed the elasticity problems for QDs, i.e., stressors, of various shapes, for various crystal symmetries (zinc-blende and wurtzite semiconductors) including the anisotropy of material properties.[25–28] The effect of coupling electric and elastic fields generated by QDs in the materials with piezoelectric response was also studied.[29] In this article, we do not include the anisotropy of the material under investigation and do not examine complex dot geometries. Rather, we employ simple models for stressor shapes and work in the framework of linear isotropic elasticity. We account for the screening influence of the free surface on the stressor elastic fields, as was proposed in Ref. 30. In Sec. II, we provide necessary relations on the elasticity of subsurface point stressors and subsurface dilatating ellipsoidal inclusions. We present a survey on the $\mathbf{k}\cdot\mathbf{p}$ approach in calculating the response of the electronic subsystem of the material on the external or internal strain.[1] The background is also devoted to the consideration of strain-induced polarization in nitride semiconductors. In the main part of the article, we develop the model for buried stressors in uniform GaN and GaN with an embedded QW. The results of the model are then presented and discussed with emphasis on the lateral change in the energy gap due to strain-induced QDs inside the QW in III-nitride binary and ternary compounds.

II. BACKGROUND

A. Elasticity of subsurface stressors

Practically all effects of QDs on the surrounding material depend on their long-range elastic field. From this point of view, an individual QD serves as a *stressor*; i.e., a source of elastic strains and stresses. The elastic field of the stressor depends on the geometry of the stressor: its volume and shape as well as the character of intrinsic distortions of the stressor, e.g., the crystal lattice mismatch between dot and matrix materials or differences in thermal expansion coefficients. Furthermore the elastic field depends on the elastic properties both inside the stressor material and the surrounding matrix as well as the position of the stressor with respect to interfaces and free surfaces. Independent of quantum dot applications, the mechanical properties of stressors were extensively studied in solid mechanics starting with Eshelby's work on elastic inclusions.[31,32]

A complete solution of the elasticity problem in the most general case of stressors in closed analytical form is not possible. For problems related to QDs, three main methods have been applied to determine the elastic behavior of the stressor: (i) theory of elastic inclusions based on exact or approximate analytical solutions of elasticity equations ("Eshelby-like" or related approaches),[11,14,23,25,30] (ii) finite element methods (FEM),[27,30,33,34] and (iii) atomistic modeling.[35,36] Approaches (i) to (iii) all have their particular advantages and disadvantages. FEM is very effective for specific cases but does not provide general solutions, and is furthermore affected by choice of boundary conditions for the modeling domain. Atomistic models require accurate interatomic potentials and are further restricted to small systems of atoms in comparison with dot sizes and the surrounding matrix.

The theory of elastic inclusions provides integral expressions for elastic fields, which can be expressed in closed analytical form in special cases, e.g., relatively simple inclusion shapes in elastically isotropic media. In many cases, it is sufficient to apply such a simplified description. In this article, we utilize two analytic approaches in stressor mechanics, which include the effect of the free surface and the dot

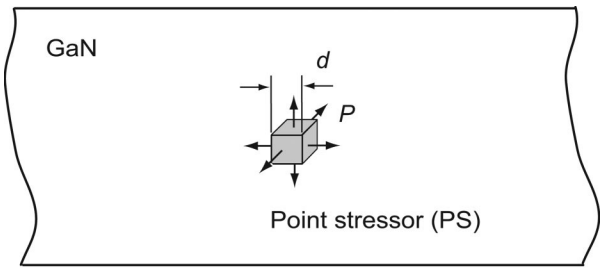

(a)

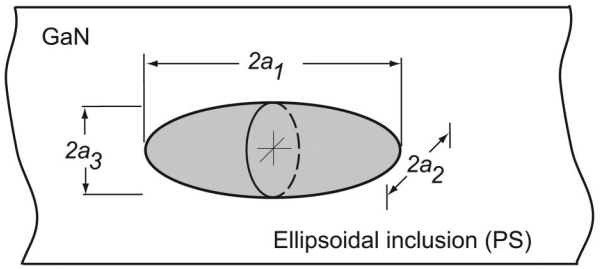

(b)

FIG. 2. The models proposed for analytical treatment of subsurface stressors in GaN. (a) Schematic for a PS placed in a GaN layer. The PS is described by three orthogonal force dipoles with separation d and magnitude P acting on the faces of a cube with volume d^3 in the limit of $d\to 0$. (b) Dilatating oblate EI with volume $V=\frac{4}{3}\pi a_1^2 a_3$ and mismatch f with respect to the surrounding material. Two of three principal diameters of the ellipsoid are assumed to be equal; i.e., $a_2=a_1$.

shape: a *point stressor* (PS) and a dilatating *ellipsoidal inclusion* (EI), which are shown schematically in Fig. 2.

In the application to semiconductor QDs, stressors originate from the crystal lattice mismatch, which can be described with the help of the misfit parameter

$$f=\frac{a_m-a_d}{a_d}, \tag{1}$$

where a_d and a_m are crystal lattice parameters for dot and matrix materials, respectively. Here, we assume isotropic mismatches; i.e., the misfit f is the same in three orthogonal directions. This assumption defines a so-called dilatating stressor, since the dilation (relative change of the volume) inside the stressor is $3f$. Distortions in the surrounding matrix also increase with stressor volume V. Therefore, stressors can be characterized by their strength $S=fV$. In the following presentation, we will employ the strength S as the main parameter for the dilatating stressor.

The simplest approach to express the far field of dilatating stressors is to ignore their geometry altogether, and to consider them as point sources of dilatation [see Fig. 2(a)] of given effective strength S; i.e., to consider them as PSs. The stresses $\sigma_{ij}^{\mathrm{PS}}$ due to a PS can be found by combining the stresses of point force dipoles. Note that if the response of a body to a point force (i.e., Green's function) is known, the elastic fields caused by any distribution of forces can be obtained by linear superposition.[37] In the case of a PS of expansion, three mutually perpendicular pairs of forces (each pair consists of a dipole of opposing forces of magnitude P, separated by a distance d along their mutual line of action) may be used [see Fig. 2(a)]. Throughout this article, we refer to such a stressor as *positive* PS (i.e., a positive stressor itself would have a larger lattice constant than the surrounding matrix). If one considers a cube of volume $V=d^3$, the average stress in the cube is P/d^2, which in turn can be related to the strains arising from the misfit f via Hooke's law. Based on such considerations, one can relate the PS strength to P and d, as

$$S^{\mathrm{PS}}=\frac{Pd}{2G}\frac{1-2\nu}{1+\nu}, \tag{2}$$

where G is the isotropic material shear modulus and ν is Poisson's ratio. By taking the limit as $d\to 0$, maintaining Pd constant, the complete elastic field for a positive PS of expansion with given strength S may be determined. The analytic form for the elastic fields of the PS exists in all those cases when Green's function has a closed solution. The stresses $\sigma_{ij}^{\mathrm{PS}}$ for a PS placed at the distance h away from the free surface of an isotropic half-space are given in the Appendix [see Eq. (A1)]. The strain components $\varepsilon_{ij}^{\mathrm{PS}}$ can be found from stresses by applying Hooke's law [Eq. (A4)]. For example, the important hydrostatic strain component $\varepsilon_{\mathrm{hydro}}^{\mathrm{PS}}(r,z)=\varepsilon_{ii}^{\mathrm{PS}}=\Sigma_{i=1}^{3}\varepsilon_{ii}^{\mathrm{PS}}$ of the subsurface PS can be obtained with the help of Eq. (A5), and it is equal to

$$\varepsilon_{\mathrm{hydro}}^{\mathrm{PS}}(r,z)=S\frac{(1+\nu)(1-2\nu)}{\pi(1-\nu)}\frac{2(z+h)^2-r^2}{[r^2+(z+h)^2]^{5/2}}, \tag{3}$$

where the cylindrical coordinates (r,z) are used (note that z is identical to x_3 defined in the Appendix). The plot of $\varepsilon_{\mathrm{hydro}}^{\mathrm{PS}}(r,z)$ is given in Fig. 3(a). Due to the presence of the free surface, the hydrostatic strain field *does not vanish* for the subsurface PS. This property is in contrast to the case of a PS in an infinite isotropic medium and it has important consequences for strain induced changes in the conduction band (see the subsequent presentation).

In the near field, strains and stresses diverge in the PS model; therefore, a more accurate approximation is required. To take into account the stressor proximity effects in an analytical treatment, we will consider a dilatating EI, as shown schematically in Fig. 2(b). In general, the elastic fields of an arbitrarily shaped dilatating inclusion can be determined by integrating the corresponding elastic fields for a PS; i.e., by distributing PSs over the finite volume of the inclusion. In the case of an EI, the stresses $\sigma_{ij}^{\mathrm{EI}}(\mathbf{r})$ outside the inclusion can be found by integration of PS stresses over the ellipsoid interior V^{EI}:

$$\sigma_{ij}^{\mathrm{EI}}(\mathbf{r})=\int_{V^{\mathrm{EI}}}\frac{1}{V^{\mathrm{PS}}}\sigma_{ij}^{\mathrm{PS}}(\mathbf{r}-\mathbf{r}')dV'. \tag{4}$$

The results of the evaluation of the Eq. 4 are given in the Appendix. In the examples to follow we discuss an oblate spheroid (EI with two equal semi-axes $a_1=a_2>a_3$) at a depth h from the surface. The strength of such a stressor is given by

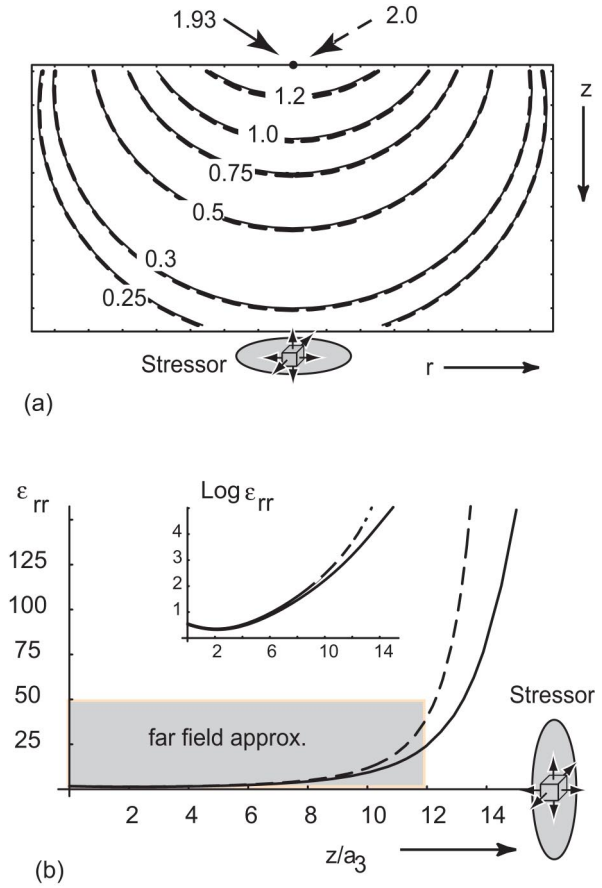

FIG. 3. Comparison of point versus ellipsoidal stressor. (a) Hydrostatic strain (dilatation field) $\varepsilon_{ii}(r,z)$ induced by the subsurface stressors. The strain is given in units of $(S/\pi h^3)[(1+\nu)(1-2\nu)]/(1-\nu)$, where S is the effective strength of the stressor placed at the distance h from the free surface of an isotropic half-space and ν is Poisson's ratio. (b) Dependence of the radial strain $\varepsilon_{rr}(0,z)$ on depth in the GaN layer. The stressor (EI or PS) is located at a distance $h=41$ nm from the surface and has effective strength $S=fV$ equivalent to an $In_{0.5}Ga_{0.5}N$ inclusion with a volume of 200π nm^3 and $f=0.051$. The strain is normalized by 1.26×10^{-4}, which corresponds to an effective Poisson ratio $\overline{\nu}=0.234$ for GaN. Results for ellipsoidal and point stressors are shown by solid and dashed lines, respectively.

$$S^{\mathrm{EI}} = \tfrac{4}{3} f \pi a_1^2 a_3. \tag{5}$$

The expressions for stress and strain in this case [see Eqs. (A7) and (A4)] are more cumbersome than those for the PS. However, a more realistic idealization of the stressor geometry is achieved. Thus, using these expressions, we can analyze the near-field effects and also consider the influence of the aspect ratio of the stressor.

A comparison of exact analytical solutions is given in Fig. 3 for both the EI and PS placed at the same distance h from the free surface and both with the same effective strength $S^{\mathrm{EI}}=S^{\mathrm{PS}}=S$. The dilatation field $\varepsilon_{kk}^{\mathrm{EI}}$ of the EI [Fig. 3(a)] agrees extremely well with the corresponding dependence for the PS. In the absence of the free surface, the dilatation outside the EI vanishes as originally, shown by Eshelby.[31] The individual components of strain and stresses in the far field also demonstrate a remarkable agreement as seen in the Fig. 3(b), where the dependencies of radial strains on z are plotted. In the near field (close to the stressor), there is a quantitative difference between the predictions of the two models. The more realistic EI model shows finite values of strain up to the surface of the ellipsoid. Therefore, we will apply the EI description for the analysis the stressor effects in its close proximity. However, in the far field, i.e., at the distances $l>l_c\approx V^{1/3}$ (in case of not extremely elongated EI), the simpler PS solutions can be successfully used for a comprehensive analysis of stressor-induced variation of electronic properties.

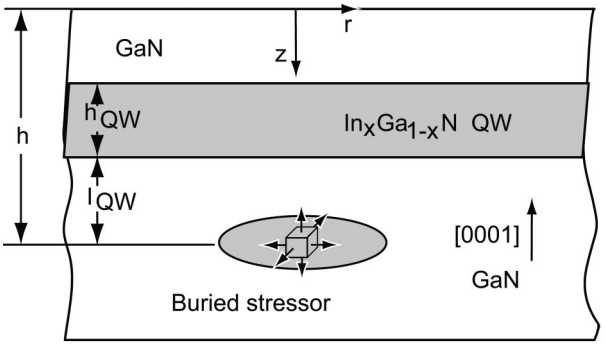

FIG. 4. Characteristic distances for a buried stressor in GaN layer with embedded QW. The sample surface $z=0$ corresponds to the (0001) GaN growth plane with the z axis in the $[000\overline{1}]$ crystallographic direction.

B. Conduction and valence band changes in the presence of strain

Mechanical strains, i.e., deviations of the unit cell from its geometry in the unstrained crystal, also modify the band structure of semiconductors. For example, the band gap of a semiconductor increases upon hydrostatic compression.[38,39] Commonly, the effects of strain on the band structure can be described using the Bir–Pikus approach,[1] which utilizes the $\mathbf{k}\cdot\mathbf{p}$ perturbation theory formalism in order to determine the deviations of the energy bands from those in the unstrained crystal. The $\mathbf{k}\cdot\mathbf{p}$ perturbation theory formalism is based on Bloch wave solutions of the Schrödinger equation of the form $\psi_{n\mathbf{k}}(r)=u_{n\mathbf{k}}(\mathbf{r})\exp(i\mathbf{k}\cdot\mathbf{r})$, where n and $\mathbf{k}$ are the band index and the electron wave vector, respectively. Substituting these Bloch functions into the Schrödinger equation, one can show that the Hamiltonian operator for the unit cell wave functions $u_{n\mathbf{k}}(\mathbf{r})$ can be written as the sum of the Hamiltonian operator for $\mathbf{k}=0$ and a term proportional to $\mathbf{k}\cdot\mathbf{p}$, with $\mathbf{p}=(\hbar/i)\nabla$. Furthermore, the eigenfunctions $u_{n0}(\mathbf{r})$, i.e., for $\mathbf{k}=0$, form a complete set of eigenfunctions such that all $u_{n\mathbf{k}}(\mathbf{r})$ may be written as a linear combination of all $u_{n0}(\mathbf{r})$, also known as the *Luttinger–Kohn representation*.[1] Hence, one can apply first-order perturbation theory with a perturbation $\mathbf{k}\cdot\mathbf{p}$ and a basis $u_{n0}(\mathbf{r})$ to investigate the band structure in the vicinity of $\mathbf{k}=0$. The new eigenstates will then be the linear combination of the $u_{n0}(\mathbf{r})$. One common example is the Luttinger–Kohn model, which describes the valence band structure of common III-V semiconductors.[2] Bir and Pikus[1] showed that the form of the strain dependence of the Hamiltonian is essentially identical to the $\mathbf{k}$-dependence of the Hamiltonian. For example, a term proportional to k_xk_y corresponds to a term proportional to the strain component ε_{xy}.

In unstrained wurtzite GaN, there are three closely spaced top valence bands (VBs) at the Brillouin-zone center,

usually referred to as heavy-hole (HH), light-hole (LH), and crystal-field split-off hole (SCH).[40,41] These VB states have atomic *p*-orbital character, in contrast to the bottom conduction band (CB), which has atomic *s*-orbital character. Since the large band gap of GaN reduces the interaction of CB and VB states, the Hamiltonian for the strain dependence of the VB can be separately given by the 6×6 matrix[3]

$$H^v = \begin{bmatrix} F & 0 & -H^* & 0 & K^* & 0 \\ 0 & G & \Delta & -H^* & 0 & K^* \\ -H & \Delta & \lambda & 0 & I^* & 0 \\ 0 & -H & 0 & \lambda & \Delta & I^* \\ K & 0 & I & \Delta & G & 0 \\ 0 & K & 0 & I & 0 & F \end{bmatrix}, \tag{6}$$

with the following strain-dependent elements:

$$F = \Delta_1 + \Delta_2 + \lambda + \theta,$$

$$G = \Delta_1 + \Delta_2 + \lambda + \theta,$$

$$H = i(A_6 k_z k_+ + A_7 k_+ + D_6 \varepsilon_{z+}),$$

$$I = i(A_6 k_z k_+ - A_7 k_+ + D_6 \varepsilon_{z+}),$$

$$K = A_5 k_+^2 + D_5 \varepsilon_+,$$

$$\Delta = \sqrt{2}\Delta_3,$$

$$\lambda = A_1 k_z^2 + A_2 k_\perp^2 + D_1 \varepsilon_{zz} + D_2(\varepsilon_{xx} + \varepsilon_{yy}),$$

$$\theta = A_3 k_z^2 + A_4 k_\perp^2 + D_3 \varepsilon_{zz} + D_4(\varepsilon_{xx} + \varepsilon_{yy}),$$

$$\varepsilon_+ = \varepsilon_{xx} - \varepsilon_{yy} + 2i\varepsilon_{xy},$$

$$\varepsilon_{z+} = \varepsilon_{xz} + i\varepsilon_{yz},$$

$$k_+ = k_x + ik_y,$$

$$k_\perp^2 = k_x^2 + k_y^2$$

The parameters D_j ($j=1$ to 6) are the deformation potentials for the VB, and A_j ($j=1$ to 7) are equivalent to the Luttinger parameters (see Ref. 40 for details) and determine the hole effective masses; ε_{lm} and k_l ($l,m=x,y,z$) are the strain and wave vector components, respectively. Δ_1 is the crystal-field parameter, while Δ_2 and Δ_3 are the spin-orbit energy parameters. The basis for H^v is given by the usual choice $(1/\sqrt{2})|X+iY,\alpha\rangle$, $(1/\sqrt{2})|X+iY,\beta\rangle$, $|Z,\alpha\rangle$, $|Z,\beta\rangle$, $(1/\sqrt{2})|X-iY,\alpha\rangle$, $(1/\sqrt{2})|X-iY,\beta\rangle$. Here, $|X\rangle$, $|Y\rangle$, and $|Z\rangle$ have the symmetry properties of the atomic p_x, p_y, and p_z orbital functions. $|\alpha\rangle$ and $|\beta\rangle$ denote the spin wave functions corresponding to spin up and spin down respectively. The diagonalization of the matrix [Eq. (6)] yields the three distinct VB maxima $E_{v,j}$.

The Hamiltonian for the strain dependence of the CB minimum is given by a 2×2 matrix with basis $|S,\alpha\rangle$ and $|S,\beta\rangle$. The eigenvalue of the Hamiltonian can be expressed by

$$E_c = \alpha\varepsilon_{zz} + \alpha_\perp(\varepsilon_{xx} + \varepsilon_{yy}) + \frac{\hbar^2 k_z^2}{2m_e} + \frac{\hbar^2 k_\perp^2}{2m_{e\perp}}, \tag{7}$$

where $\alpha_\perp$, $\alpha_\parallel$ and $m_{e\parallel}$, $m_{e\perp}$ denote the CB deformation potentials and electron effective mass, respectively. Since in the following analysis we will be only interested in the ground-state energies ($\mathbf{k}=0$), we will find that Eqs. (6) and (7) are substantially simplified.

C. Polarization effects in nitride semiconductors

A sizable redshift of the ground-level transitions of wurtzite nitride semiconductor quantum wells has been observed by various groups[42–45] for increasing well width. This phenomenon is sometimes accompanied by the concomitant reduction of the oscillator strength and by the increase of the decay time of the transition. All together, these effects point towards the existence of strong built-in electrostatic fields in wurtzite nitride semiconductors, which causes a substantial QCSE.[3] The underlying phenomenon is the presence of large electrical polarization fields in wurtzite nitride semiconductors: the spontaneous polarizations are of the same order of magnitude as those of ferroelectrics.[46] As we already mentioned Sec. I, the magnitude of the piezoelectric constants considerably exceeds that of other III-V semiconductors.

The presence of polarization is strongly connected to the unit cell symmetry of a crystal. Nitride semiconductors exist in both the zinc-blende and wurtzite structures. In both cases, each group-III atom is tetrahedrally coordinated to four nitrogen atoms. The main difference between these two structures is the stacking sequence of close packed diatomic planes. These stacking sequences are ABABAB along the wurtzite {0001} directions and ABCABC along the zinc-blende {111} directions. This difference in stacking sequence results in distinct space group symmetries: $P6_3mc$ for wurtzite and $F\bar{4}3m$ for zincblende.

In the absence of external electric fields, the total macroscopic polarization **P** of a solid is the sum of the spontaneous polarization of the equilibrium structure and of the strain-induced, piezoelectric polarization.The zinc-blende compound semiconductors such as GaAs and InP have four symmetry equivalent polar $\langle111\rangle$ axes whose contributions cancel each other in equilibrium. Hence, these materials are free of electrical polarization at equilibrium. In contrast, the wurtzite phase has a singular polar axis, namely, the [0001] axis. Thus, the wurtzite phase has a spontaneous electrical polarization parallel to the [0001] direction even at equilibrium.

In practice, semiconductor layers are often grown under strain due to the lattice mismatch with the underlying substrate. Such deformations of the unit cell can lead to additional piezoelectric polarization. The presence of this kind of polarization is again closely related to the unit cell symmetry; namely, to the lack of inversion symmetry. The contributions of the four polar axes of zinc-blende structures cancel each other for growth along a $\langle001\rangle$ direction. However, growth along one of the polar axes reduces the symmetry and the crystal exhibits piezoelectric polarization. In contrast, the wurtzite structure with its unique polar [0001] axis

always carries piezoelectric polarization for any growth direction. The total electric polarization **P** is the sum of spontaneous polarization $\mathbf{P}_{sp}$ and piezoelectric polarization $\mathbf{P}_{pz}$.

In general, the elementary cell of material under consideration can be subjected to an arbitrary strain ε_{ij}. By taking into account the symmetry of the space group $P6_3mc$ of wurtzite GaN, the piezoelectric polarization is related to strains as:[47]

$$\mathbf{P}_{pz} = \begin{pmatrix} 0 & 0 & 0 & 0 & e_{15} & 0 \\ 0 & 0 & 0 & e_{15} & 0 & 0 \\ e_{31} & e_{31} & e_{33} & 0 & 0 & 0 \end{pmatrix} \begin{pmatrix} \varepsilon_{xx} \\ \varepsilon_{yy} \\ \varepsilon_{zz} \\ \varepsilon_{yz} \\ \varepsilon_{xz} \\ \varepsilon_{xy} \end{pmatrix}, \tag{8}$$

with the elements e_{ij} of the piezoelectric tensor in Voigt notation.[48]

Any spatial change in total polarization **P** leads to a fixed charge $\rho = -\nabla \cdot \mathbf{P}$. Prime examples are two-dimensional electron gases at (Al,Ga)N/GaN interfaces and alternating sheet charge in QWs, giving rise to the QCSE.[3,49] In the following analysis, we will calculate the distribution of fixed charges induced by subsurface stressors.

III. DESCRIPTION OF THE MODEL

In our model, shown schematically in Fig. 4, the dilatation stressor is located at $r=(x^2+y^2)^{1/2}=0$ and $z=h$. The material surrounding the stressor is considered either to be a uniform GaN matrix or a GaN/In_xGa_{1-x}N/GaN single QW that is grown pseudomorphically between the stressor and the free surface. The designations for the characteristic lengths h, h_{QW}, and l_{QW} are also shown in the Fig. 4. The $z=0$ plane is taken as the (0001) sample surface and the z axis points into the sample; hence, the z axis is parallel to $[000\bar{1}]$. As we already discussed in Sec. II A, the elastic properties of a medium are, in general, anisotropic, and the stressor may have arbitrary shape and size, leading to a complex elastic field in close vicinity to the stressor, thus requiring rather elaborate analytical or FEM calculations. To simplify the model and to proceed with analytically tractable results, the following approximations were employed: (i) the stressor is taken as either a PS or a dilatation EI, (ii) the same elastic constants were used for (In,Ga)N and GaN, and (iii) isotropic elasticity is used with an effective Poisson's ratio and shear modulus, which are derived from anisotropic elastic constants of GaN (see the Appendix for details). We note that the EI provides a good approximation for the elastic fields of inclusions with more complex shapes.[30] Additionally, since the QW alloys are relatively dilute (we will treat $In_xGa_{1-x}N$ with $x=0.05$ or 0.15), we believe that we were justified in assuming the same elastic constants for the matrix and wells.

As shown in Sec. II, the strength of the stressor can be defined via $S=fV$, where V is the stressor volume and f is the crystal lattice mismatch between material of the stressor and surrounding material. The volume of the stressor can be directly estimated from the experimental data of QD structures in III-nitride semiconductors.[4,50] We consider QDs embedded in a GaN matrix with typical dot dimensions of around 20 nm as a lateral size in the basal plane and a height along the z axis of approximately 2 nm, similar to recently reported GaN dots in an AlN matrix.[50] For simplicity, we prescribe a volume of 200π nm^3 to the stressor. In our numerical examples we will always use this value for V.

TABLE II. Crystal lattice parameters of III-nitrides with wurtzite structure (Refs. 52 and 59).

Lattice parameters	AlN	GaN	InN
a (Å)	3.112	3.189	3.54
c (Å)	4.982	5.185	5.705

The effective misfit parameter f for wurtzite semiconductors can be estimated by taking into account the difference in crystal lattice translations in the basal plane and in the z-axis direction. The lattice parameters of III-nitrides are given in Table II. For such materials, one can introduce a pair of misfit parameters f_a and f_c, given by

$$f_a = \frac{a_m - a_d}{a_d}, \tag{9a}$$

$$f_c = \frac{c_m - c_d}{c_d}, \tag{9b}$$

where a_m, a_d, and c_m, c_d are the a and c wurtzite lattice parameters of the matrix and the dot, respectively. The effective stressor/matrix mismatch can then be defined as

$$f = \frac{2f_a + f_c}{3}. \tag{10}$$

The results of Eq. (10) are summarized in Table III for a number of possible combinations of the dot and matrix materials. One can see that for III-nitrides both positive ($f>0$) and negative ($f<0$) stressors can be realized (at least hypothetically).

After the strength of the stressor is determined via the effective misfit f and the effective volume V, the elastic field $\varepsilon_{ij}^{stressor}$ induced in the matrix by the stressor is found by applying the formulas for PS and EI described in Sec. II. As it follows from the analysis for the case of elastic isotropy, the only material parameter appearing in the stressor strain distributions is Poisson's ratio. Since wurtzite GaN is elastically anisotropic, we choose to use an effective Poisson's ratio $\bar{\nu}$ [given by Eq. (A18)], which was derived by averag-

TABLE III. Effective lattice mismatch for wurtzite III-nitrides.

Material		Misfit parameter
Stressor	Matrix	f
GaN	AlN	0.029
InN	GaN	0.096
$In_{0.5}Ga_{0.5}N$	GaN	0.051
AlN	GaN	−0.030

TABLE IV. Band structure parameters of wurtzite GaN.

Parameters	Set I, Ref. 3 (eV)	Set II, Ref. 52 (eV)	Set III, Ref. 53 (eV)
Δ_1	0.022	0.010	⋯
Δ_2	0.005	0.017	⋯
$\alpha_\parallel$	−45.5	−8.6	−6.0
$\alpha_\perp$	−44.5	−6.8	−6.0
D_1	−41.4	−3.7	0.11
D_2	−33.3	4.5	5.54
D_3	8.2	8.2	5.76
D_4	−4.1	−4.1	−3.04
D_5	−4.7	−4.0	⋯
D_6	$D_6=(D_3+4D_5)/\sqrt{2}$ (see Ref. 40, and references therein).		

ing Poisson's ratios along the three mutually perpendicular axes chosen in characteristic crystallographic directions, as

$$\overline{\nu} = -\frac{1}{3}\left(\frac{s_{13}}{s_{33}} + \frac{s_{12}+s_{13}}{s_{11}}\right). \tag{11}$$

where s_{ij} are the elastic compliances for GaN. Using the elastic constants from Ref. 51 we obtain $\overline{\nu}=0.234$.

When a pseudomorphically grown single QW is considered, additional uniform strains $\varepsilon_{ij}^{\mathrm{QW}}$ are generated inside the well, given by

$$\varepsilon_{xx}^{\mathrm{QW}} = \varepsilon_{yy}^{\mathrm{QW}} = f_{\mathrm{QW}}, \tag{12a}$$

$$\varepsilon_{zz}^{\mathrm{QW}} = -\frac{2\overline{\nu}}{1-\overline{\nu}} f_{\mathrm{QW}}, \tag{12b}$$

where the misfit parameter for the QW f_{QW} is defined as

$$f_{\mathrm{QW}} = \frac{a_m - a_{\mathrm{QW}}}{a_{\mathrm{QW}}}. \tag{13}$$

The in-plane lattice parameter a_{QW} of the QW material with the composition $In_xGa_{1-x}N$ can be found in accordance with the Vegard's law:

$$a_{\mathrm{QW}} = x a_{\mathrm{InN}} + (1-x) a_{\mathrm{GaN}}. \tag{14}$$

Using Eqs. (13) and (14) and taking into account the data for the lattice parameters of GaN and InN (Table II), we obtain $f_{\mathrm{QW}}=-0.016$ and -0.0055 for In content of $x=0.15$ and 0.05, respectively.

Finally, the combined action of the stressor and the QW is given by the superposition of the corresponding elastic strains:

$$\varepsilon_{ij}^{\mathrm{total}} = \varepsilon_{ij}^{\mathrm{stressor}} + \varepsilon_{ij}^{\mathrm{QW}}. \tag{15}$$

To evaluate the influence of the stressor on the material electronic properties, we apply a $\mathbf{k}\cdot\mathbf{p}$ approach as presented in Sec. II. For deformation potentials of GaN we use set I from Table IV, which corresponds to parameters utilized in our preliminary publication.[25] Because the data on deformation potentials for wurtzite III-nitrides are diverse, we also have checked different sets of values, which are also included as set II and set III in Table IV. Set II is recommended band structure parameters from a recent review article by Vurgaftman and Meyer[52] and set III represents the data used by Van de Walle in his study of "absolute" deformation potentials and the band offsets at wurtzite III-nitrides heterojunctions.[53] We note that in spite of distinctly different values of the individual deformation potentials, all three sets provide comparable values for interband deformation potentials, i.e., $a_1=\alpha_\parallel-D_1$ and $a_2=\alpha_\perp-D_2$. It also will be shown in the next section that all the sets of parameters have similar effects on the band edge shifts in III-nitrides induced by subsurface stressors.

For the analysis of the stressor-induced polarization charges we use the following values of the piezoelectric coefficient for GaN: $e_{33}=0.73\ \mathrm{C\,m^{-2}}$, $e_{31}=-0.49\ \mathrm{C\,m^{-2}}$,[54] and $e_{15}=-0.40\ \mathrm{C\,m^{-2}}$, where the value of the coefficient e_{15} is the estimate obtained on the averaging the data reported in Refs. 23 and 55.

IV. STRESSOR-INDUCED BAND EDGE SHIFTS

The change of the VB structure is *nonlinear* with strain as these energies represent the eigenvalues of a 6×6 Hamiltonian in the $\mathbf{k}\cdot\mathbf{p}$ calculations (see Sec. II for details). We will examine the shifts of the CB and VB edges due to the subsurface stressor strain field by utilizing the $\mathbf{k}\cdot\mathbf{p}$ perturbation approach developed by Bir and Pikus,[1] and employing the corresponding deformation potentials for GaN.[3] Due to strain, both the CB and the VB states, i.e., HH, LH, and SCH, are modified leading to shifts of the corresponding band edges relative to their values for unstrained material. The stressor strain field leads to changes in the original VB states such that it is no longer correct to simply describe them as HH, LH, and SCH.[24] Therefore, we label the individual VBs as top, middle, and bottom VB according to their energy, with the top VB being closest to the CB.

The shifts of the CB energies E_c^{def} in a uniform GaN matrix due to positive and negative subsurface PSs are shown in Fig. 5. We use parameters for the PSs that are equivalent in the far field to $In_{0.5}Ga_{0.5}N$ and AlN QDs with misfit parameters $f=0.051$ and $f=-0.030$, respectively. All the results shown for the PS are calculated within the valid range of the point source approximation as we do not approach the point source closer than its characteristic length l_c. The shift of the CB is proportional to the hydrostatic strain [e.g., see Eq. (7) in Sec. II]; hence, Fig. 5 resembles Fig. 3(a) in different units. We see that either a positive or negative PS leads to only slight changes in the CB energy in the subsurface region above the stressor. In contrast, the changes in the VB energies E_v^{def} (induced by PSs and shown in Fig. 6) show a rather complex dependence on the actual location. In-plane and out-of-plane cross sections of the VB structure are shown along the z axis and for two different depths z in Figs. 6(a)–6(c), respectively. In Fig. 6, the left column gives results for the positive PS, whereas the right column provides the results for the negative PS. The lower part of the figure [Fig. 6(d)] presents results for the other set of band structure parameters; namely, set II from Table IV. Near the surface, the VBs have relative separations only slightly different from the values of unstrained material [see Fig. 6(a)]. However, in the case of the positive PS, with increasing depth z, the separation of the top and middle VBs decreases until they cross

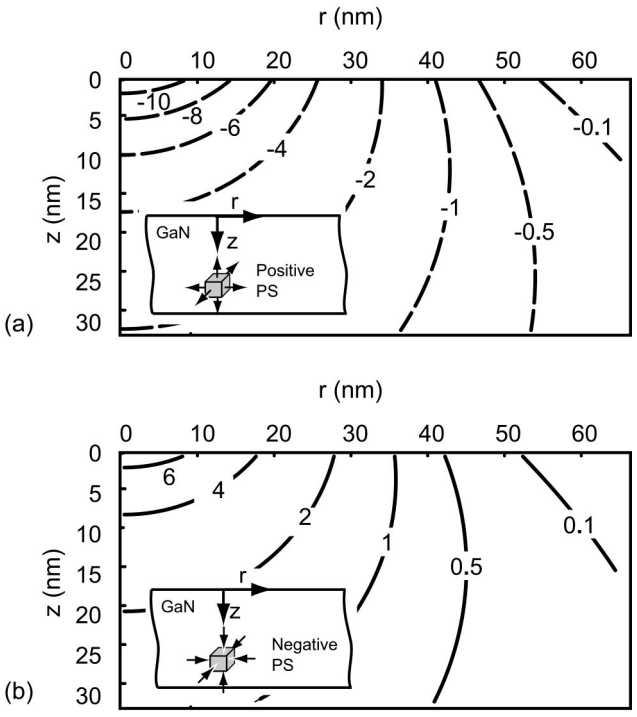

FIG. 5. Map for GaN CB edge changes E_c^{def} due to strain fields of buried stressors. (a) For the positive PS with effective strength $S=fV$ equivalent to an $In_{0.5}Ga_{0.5}N$ inclusion with a volume of 200π nm^3 and $f=0.051$. (b) For the negative PS with effective strength $S=fV$ equivalent to an AlN inclusion with a volume of 200π nm^3 and $f=-0.030$. The stressors are located at a distance $h=41$ nm from the surface The effective Poisson's ratio was taken as $\bar{\nu}=0.234$, the contour values are given in meV.

(at $z\approx 25$ nm for the parameters used for Fig. 6). Finally, the top VB moves towards the CB, while the other two VBs bend away from the CB, maintaining their separation. For the negative PS such a behavior is not observed; in this case no crossing occurs, but both the top and the middle VBs move towards the CB when approaching the negative PS.

It follows from Figs. 6(b) and 6(c) (left and right), for $r>h$, that the VBs are only weakly affected by the presence of the stressor regardless of the depth z. Close to the sample surface [Fig. 6(b)], the relative positions of the VBs change only slightly close to the symmetry axis. This influence is due to the hydrostatic component of the strain tensor. When approaching the stressor [see Fig. 6(c)], its effect becomes visible even still inside the region of the far-field approximation. The remarkable feature of the PS influence on the VB structure is the unidirectional effect of positive and negative stressors. Both types of stressor raise the top VB level.

It is clear from the comparison of the Figs. 6(c) and 6(d) that the use of the different set of deformation potential parameters (i.e., set II instead set I) does not change the main conclusion on the character of the stressor influence on the shift of the VB edge. The same observation was also obtained for the parameters of set III from the Table IV. Therefore, all the following reported results were obtained by using the deformation potential parameters of set I.

It is interesting to consider the case of a $GaN/In_xGa_{1-x}N/GaN$ QW structure, which will provide vertical confinement of the carriers. The total strain field from Eq. (15) was used as input for the Hamiltonian in the $\mathbf{k}\cdot\mathbf{p}$ calculations. For a positive stressor, we obtained a CB potential exhibiting lateral electron confinement at $r=0$ regardless of the actual depth of the QW. However, holes will be either trapped away or at $r=0$ depending on the actual location of the well. Therefore, we identify two important possibilities. For a shallow well close to the surface, electrons and holes show significant lateral separation and thus would have low radiative recombination rates. However, for a QW sufficiently close to the stressor, both electrons and holes may be trapped at $r=0$ in such a way that they are spatially localized resulting in a strain-induced QD inside the QW. To investigate this effect in detail, we use an EI instead of a PS since the QW may stay in close proximity to a stressor.

Figure 7 provides the results of the VB calculations for an EI placed at the depth $h=41$ nm in a GaN matrix with an additional QW characterized by $h_{\mathrm{QW}}=3$ nm, and $l_{\mathrm{QW}}=4$ nm. The material for the EI was chosen to be either $In_{0.5}Ga_{0.5}N$ (positive stressor with $f=0.051$) or AlN (negative stressor with $f=-0.030$); the volume of the EI was taken as $V=200\pi$ nm^3. The material in the $In_xGa_{1-x}N$ QW corresponds to either $x=0.05$ (moderate strained well) or $x=0.15$ (strongly strained well). From the analysis of the plots, we may see the difference regarding the results obtained for the point stressor. In the case of positive EI, the local minimum in the VB profile emerges just above the center of the ellipsoid; i.e., at $r=0$. For a strongly strained QW, the minimum can be even lower than the far-field (large r) VB energy level, as shown in Fig. 7(b). At the same time, there is a pronounced maximum of the order of 50 to 100 meV shifted towards the ends of ellipsoid. For a negative EI, the top VB has the maximum above the inclusion center. The characteristic change in E_v^{def} with respect to the values for the QW in the absence of the stressor is $\sim$50 meV.

In the general case, from our simplified description we cannot predict the exact positions of VB and CB edges, but can provide only relative change in their energy due to deformation effects. Useful information, however, can be obtained for the change of the energy gap ΔE_g in strain-induced QD, as is presented in Fig. 8. In the z direction there is a sharp change of ΔE_g, which is caused mainly by the chemical composition and uniform strain inside the QW. This effect is combined with the effect of the stressor. In the r direction, the influence of the nonuniform strain of the EI manifests itself more clearly. For example, the negative stressor [see Fig. 8(b) right] demonstrates the nonuniform strain-related reduction of the band gap of the order of 50 meV. To calibrate the results of the calculations, we utilized the following value for the gap change in the strained $In_{0.15}Ga_{0.85}N$ QW: $\Delta E_g^{\mathrm{QW}}=-0.61$ eV. This value was obtained by extrapolating the experimentally found coefficient $dE_g/dx=-4.1$ eV for pseudomorphically strained $In_xGa_{1-x}N$ layers.[56] It is clear from Fig. 8(b) that negative stressors in the vicinity of QWs can give rise to strain-induced dots within the wells.

V. STRESSOR-INDUCED POLARIZATION CHARGES

The density of fixed polarization charges in the system with the stressor is related to local variations of the total

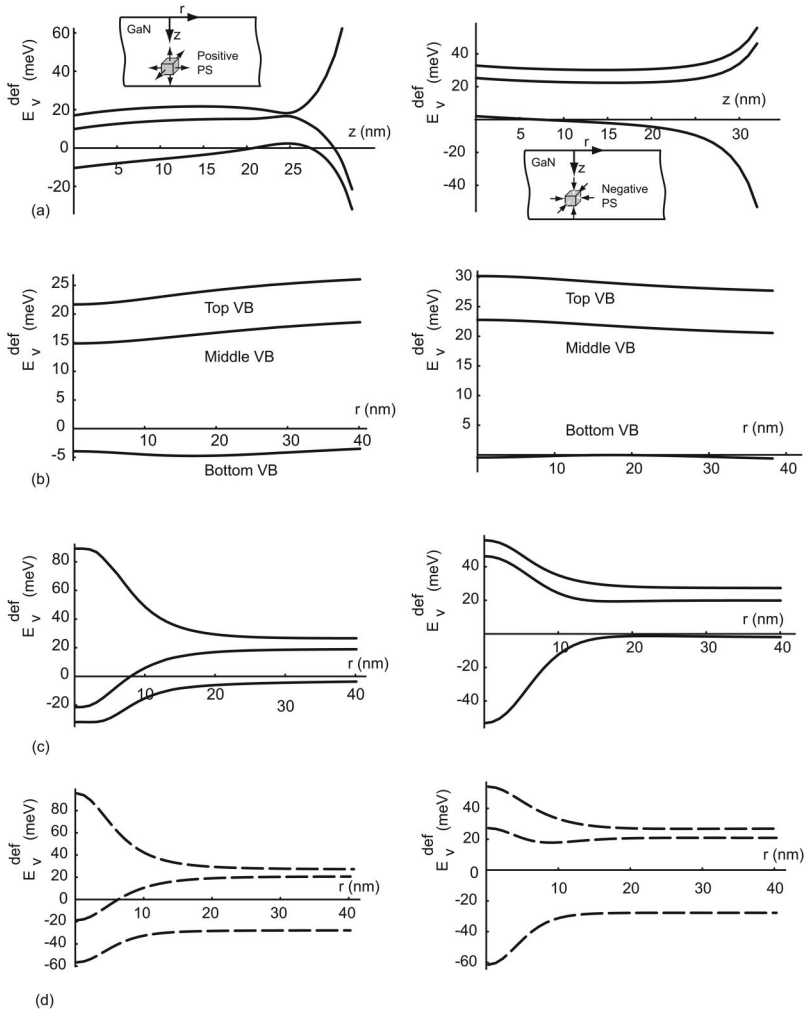

FIG. 6. Strain-induced change E_v^{def} in the VB structure of GaN due to the presence of the subsurface point stressors. (a) Dependence of the VB maxima on depth z for $r=0$. (b), (c), and (d) Radial dependencies for the energy of VBs for $z=15$, $z=33$, and $z=33$ nm (set II), respectively. Results for parts (a), (b), and (c) were obtained for deformation potential parameters from set I, and results for (d) were obtained for deformation potential parameters from set II. VBs are designated as top, middle, and bottom ones. (top closest to the CB). The left column presents the results for positive PS, with the effective strength S equivalent to $In_{0.5}Ga_{0.5}N$ inclusion with a volume of 200π nm^3 and $f=0.051$. The right column presents the results for negative PS, with the effective strength S equivalent to AlN inclusion with a volume of 200π nm^3 and $f=-0.030$. The distance from the stressor to the layer surface is $h=41$ nm. The effective Poisson's ratio was taken as $\bar{\nu}=0.234$.

polarization **P**, which is the sum of the spontaneous and the piezoelectric polarization, $\mathbf{P}_{\mathrm{sp}}$ and $\mathbf{P}_{\mathrm{pz}}$, respectively. The spontaneous and piezoelectric polarization constants of ternary alloys are linearly interpolated between the corresponding values of the binaries. For calculating $\mathbf{P}_{\mathrm{pz}}$ we employ [see Eq. (8)] the piezoelectric tensor of wurtzite nitride semiconductors, which gives us

$$\mathbf{P}_{\mathrm{pz}} = \begin{pmatrix} e_{15}\varepsilon_{xz} \\ e_{15}\varepsilon_{yz} \\ e_{31}(\varepsilon_{xx}+\varepsilon_{yy})+e_{33}\varepsilon_{zz} \end{pmatrix}, \tag{16}$$

where the piezoelectric constants of GaN e_{31}, e_{33}, and e_{15} have the values given in Sec. III. Finally, the density of fixed polarization charges $\rho(x,y,z)$ is given by $-\nabla\cdot\mathbf{P}$.

The example of these calculations is shown in Fig. 9 for the positive stressor in the absence of a QW. The fixed charge density ρ exhibits the same symmetry as the strain field; i.e., rotational symmetry with respect to the z axis: $\rho(x,y,z)=\rho(r,z)$. This finding is due to the symmetry of the piezoelectric tensor and is in contrast to the case of a stressor in a zinc-blende crystal where the z axis has $\bar{4}$ symmetry axis for the polarization charge density, leading to a quadrupole of the fixed electric charge density.[14] As seen from Fig. 9, both positive and negative polarization charges are present. For large in-plane separations r, we have a relatively low density of negative fixed charges in the 10^{16} cm^{-3} range. As we approach the z axis, we can distinguish two regimes. Close to the surface, we have positive fixed charges in the mid- to high-10^{16} cm^{-3} range. This charge density can be easily screened by free electrons, taking into account the usually reported unintentional n-type doping level of 10^{16}–10^{17} cm^{-3} in GaN. In contrast, for larger depths, negative fixed charges are found that can be as high as in the mid-10^{18} cm^{-3} range at a distance of l_c from the stressor on the z axis.

In general, one has to combine the effects of deformation potentials and polarization charges in order to obtain self-consistent solutions for wave functions and energies of electrons and holes. Therefore, one has to solve both the Schrödinger and the Poisson equations simultaneously. This is straightforward in one dimension [see, e.g., Ref. 57], but, is a substantial numerical task in two or three dimensions. In this work, we restricted ourselves to the uncoupled effects of deformation potentials and polarization charges, but will pursue self-consistent solutions in future work.

In the absence of solutions of both the Schrödinger and the Poisson equations, we can still gain insight into the results of this work. In n-type material, the Fermi level should remain close to the CB; thus most, if not all, of the strain-induced band motion will be in the VB. A positive stressor

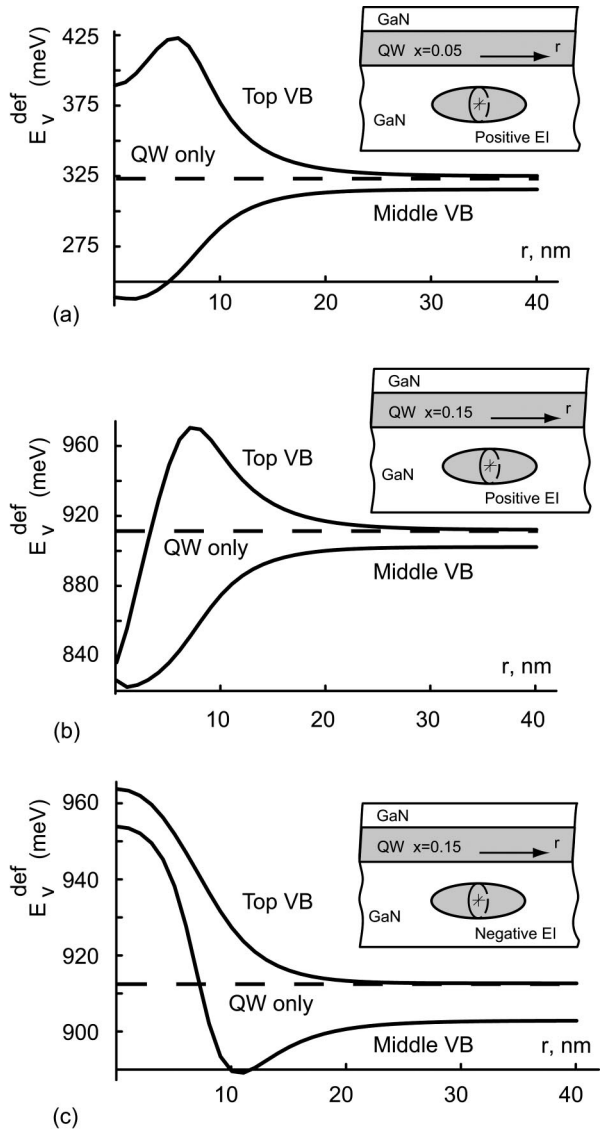

FIG. 7. Dependence of the strain-induced change E_v^{def} in the VB structure on spatial coordinates for $GaN/In_xGa_{1-x}N/GaN$ QW sandwich structure in the presence of the subsurface ellipsoidal stressors: (a) for $x=0.05$ and positive $In_{0.5}Ga_{0.5}N$ EI; (b) for $x=0.15$ and positive $In_{0.5}Ga_{0.5}N$ EI; and (c) for $x=0.15$ and negative AlN EI. Stressor parameters: volume $V=200\pi$ nm^3, aspect ratio $a_2=a_3=3$, $h=41$ nm. QW parameters: $h_{\mathrm{QW}}=3$ nm, $l_{\mathrm{QW}}=4$ nm. The effective Poisson's ratio was taken as $\bar{\nu}=0.234$. The dashed lines show the top VB level in the absence of stressor. The plots are given for the bottom of the QW as shown schematically in the inset in (b).

will give rise to a negative polarization-induced fixed charge density in the surrounding matrix (see Fig. 9) and additionally, a positive stressor in *n*-type material will cause upward motion of the VB (see Fig. 6). Thus, in *n*-type materials, excess holes, such as generated by photoexcitation or electrical injection, will be attracted to the stressor. $In_xGa_{1-x}N$ or InN dots in an *n*-type GaN matrix should be a reasonable realization of this case—the $In_xGa_{1-x}N$ dots will be a positive stressor and intentional or unintentional doping of the GaN matrix is readily achieved. Analogous arguments can be developed for negative stressors. In this case, favorable structures for *p*-type matrices with negative stressors would attract minority carriers (electrons in this case).

VI. SUMMARY AND CONCLUSIONS

We have investigated the influence of the non uniform elastic field that originates from a subsurface stressor (e.g., quantum dot) on the electronic properties of III-nitrides. Two different analytical models of subsurface stressors were explored: (i) point source of dilatation, i.e., point stressor (PS) and (ii) dilatation ellipsoidal inclusion (EI). The stressor effective strength was shown to be equal to the product of the inclusion volume V and lattice mismatch f between the materials of the inclusion and surrounding matrix. The cases of positive (e.g., $In_{0.5}Ga_{0.5}N$ inclusion, $f=0.051$) and negative (e.g., AlN inclusion, $f=-0.030$) stressors in GaN matrix have been considered. It was argued that the PS model is valid for all stressors in the far field and therefore can be applied with a good accuracy at distance $l>l_c\approx V^{1/3}$ (in case of inclusions that are not extremely elongated).

We proposed and analyzed the following material structure design: a uniform semi-infinite GaN matrix with a buried stressor or GaN matrix with a single $In_xGa_{1-x}N$ ($x=0.05$ and 0.15) QW that is grown pseudomorphically between the stressor and the free surface. The presence of the strained QW is responsible for the vertical confinement for electron and holes, whereas the presence of the buried stressor can provide lateral confinement of the carriers.

To examine the shifts of the CB and VB edges caused by the stressor, we applied a $\mathbf{k}\cdot\mathbf{p}$ perturbation theory approach with prescribed values of deformation potentials typical for III-nitrides. We found that buried stressors only affect the CB in the near-surface region. For "deep" stressors (placed at large distance) from the surface the effect is small. Significant influence has been found of stressors on the VB shift. It has been demonstrated that both negative and positive stressors cause upward motion of top VB. In the vicinity of the either an AlN or $In_{0.5}Ga_{0.5}N$ stressor, the change in energy of the top valence band can be on the order of 50 meV. Stressors in the vicinity of a QW provide the possibility for forming strain-induced QDs within the QW with lateral confinement also on the order of 50 meV.

In addition to the effect of band edge shift and the change in the energy gap via deformation potentials, subsurface stressors are responsible for the formation of polarization charges, with their distribution depending on symmetry of the piezoelectric tensor and the character of the stressor deformation field. It was shown that positive stressors with strength typical for experimentally observed in III-nitrides quantum dots give rise to large negative space charge in the vicinity of the stressor.

A complete understanding of the optical emission behavior of III-N structures should include effects of heterogeneous strain caused by composition fluctuations, dislocations, and intentional or unintentional stressors.

ACKNOWLEDGMENTS

The authors acknowledge several useful discussions with Prof. Jasprit Singh and Prof. Chris Van de Walle. This work was supported in part by AFOSR (T. Steiner and G. Witt, program managers).

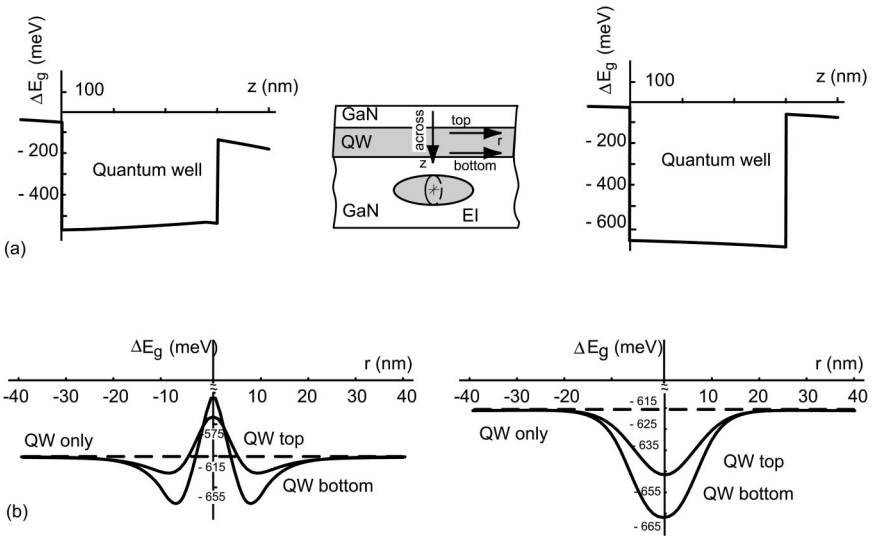

FIG. 8. Change of the band gap in $GaN/In_xGa_{1-x}N/GaN$ QW sandwich due to buried ellipsoidal stressors. (a) Band gap dependence on depth z for $r=0$. (b) Band gap dependence on the in-plane position near the top and the bottom of the QW. The left and right columns present results for positive $In_{0.5}Ga_{0.5}N$ and negative AlN EIs, respectively. Stressors parameters: volume $V=200\pi$ nm^3, aspect ratio $a_2=a_3=3$, $h=41$ nm. QW parameters: $x=0.15$, $h_{QW}=3$ nm, $l_{QW}=4$ nm. The effective Poisson's ratio was taken as $\bar{\nu}=0.234$. Dashed line shows the top VB level in the absence of stressor.

APPENDIX: STRESSES OF SUBSURFACE STRESSORS AND EFFECTIVE POISSON'S RATIO OF THE MATERIAL

Stresses for the point source of dilatation: positive PS

In the coordinate system (x_1,x_2,x_3) related to the free surface of the isotropic half-space, the PS occupies the position $(0,0,h)$. Its stresses are:[30,58]

$$\sigma_{ij}=S\frac{G(1+\nu)}{2\pi(1-\nu)}\left[\frac{\partial^2}{\partial x_i\partial x_j}\left(-\frac{1}{R_1}\right)+\nu\delta_{ij}\frac{\partial^2}{\partial x_3^2}\left(\frac{4}{R_2}\right)-x_3\frac{\partial^3}{\partial x_3\partial x_i\partial x_j}\left(\frac{2}{R_2}\right)+(-4\nu+3)(-1+\delta_{3i}+\delta_{3j})\times\frac{\partial^2}{\partial x_i\partial x_j}\left(\frac{1}{R_2}\right)-\delta_{3j}\frac{\partial^2}{\partial x_3\partial x_i}\left(\frac{1}{R_2}\right)-\delta_{3i}\frac{\partial^2}{\partial x_3\partial x_j}\left(\frac{1}{R_2}\right)\right], \tag{A1}$$

where S is the PS strength, G is the shear modulus, ν is Poisson's ratio, δ_{ij} is Kroneker delta, and $R_{1,2}=\sqrt{x_1^2+x_2^2+(x_3\mp h)^2}$. The hydrostatic pressure is defined as

$$p=-\frac{1}{3}\sigma_{kk}=-\frac{1}{3}\sum_{k=1}^{3}\sigma_{kk}, \tag{A2}$$

which gives the following result for the subsurface PS:

$$p=-\frac{2S}{3}\frac{G(1+\nu)^2}{\pi(1-\nu)}\frac{\partial^2}{\partial x_3^2}\left(\frac{1}{R_2}\right). \tag{A3}$$

Strains are related to the Hooke's law:

$$\varepsilon_{ij}=\frac{1}{2\mu}\left(\sigma_{ij}-\frac{\nu}{1+\nu}\sigma_{kk}\delta_{ij}\right). \tag{A4}$$

Local dilatation (hydrostatic strain) is expressed as

$$\varepsilon_{\text{hydro}}=\varepsilon_{ii}=\sum_{i=1}^{3}\varepsilon_{ii}=-\frac{3}{2\mu}\frac{1-2\nu}{1+\nu}p, \tag{A5}$$

where the coefficient in front of the pressure p on the right-hand side of Eq. (A5) represents the inverse bulk modulus.

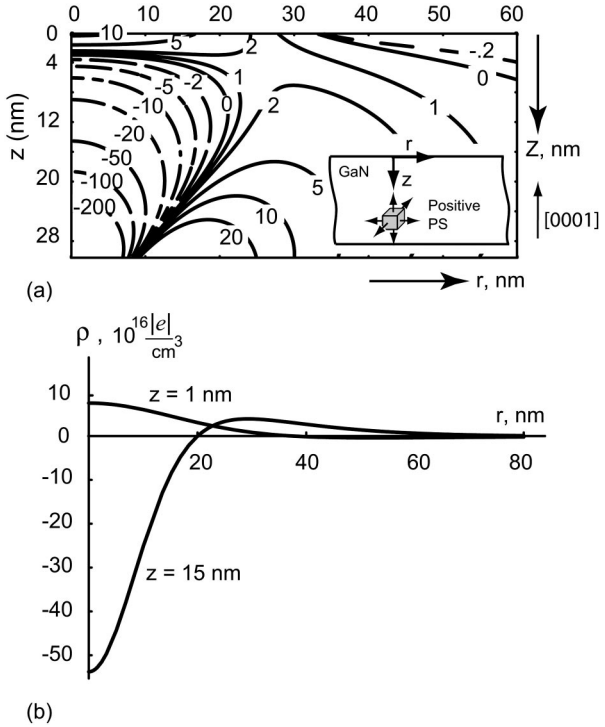

FIG. 9. Spatial dependence of the subsurface stressor induced fixed polarization charge density. (a) Map for charge distribution in GaN due to the strain field of the buried stressor; the contour values for the charge density are given in $10^{16}|e|/\text{cm}^3$. (b) Radial dependencies for the charge density for $z=1$ and $z=15$ nm, respectively. The plots were obtained for a positive PS located at a distance $h=41$ nm from the surface and with effective strength $S=fV$ equivalent to an $In_{0.5}Ga_{0.5}N$ inclusion with a volume of 200π nm^3 and $f=0.0507$. The effective Poisson's ratio was taken as $\bar{\nu}=0.234$. The piezoelectric coefficient for GaN were taken as $e_{33}=0.73$ C m^{-2}, $e_{31}=-0.49$ C m^{-2}, and $e_{15}=-0.40$ C m^{-2}.

Stresses for the dilatating ellipsoidal inclusion: positive EI

As shown by Mura,[37,58] the stress field for an EI in a half-space can be obtained by integrating the displacement field that gave rise to Eq. (A1) over the domain

$$\frac{x_1'^2}{a_1^2}+\frac{x_2'^2}{a_2^2}+\frac{(x_3'-h)^2}{a_3^2}\leqslant 1, \tag{A6}$$

where a_1, a_2, and a_3 denote the semi-axes of the ellipsoid along the respective coordinate directions, and h denotes the depth of the center of the ellipsoid from the surface. For points exterior to the inclusion, the stress components take the form

$$\sigma_{ij}=S\frac{G(1+\nu)}{2\pi(1-\nu)}\left[-\frac{\partial^2\psi}{\partial x_i\partial x_j}-x_3\frac{\partial^3\phi}{\partial x_3\partial x_i\partial x_j}+4\nu\delta_{ij}\frac{\partial^3\phi}{\partial x_3^2}-(3-4\nu)(\delta_{3i}+\delta_{3j}-1)\frac{\partial^3\phi}{\partial x_i\partial x_j}-(\delta_{3i}+\delta_{3j})\frac{\partial^3\phi}{\partial x_i\partial x_j}\right], \tag{A7}$$

where

$$\psi=\frac{3}{4}\int_{\lambda}^{\infty}\frac{1-\left(\frac{y_1^2}{a_1^2+s}+\frac{y_2^2}{a_2^2+s}+\frac{y_3^2}{a_3^2+s}\right)}{\sqrt{(a_1^2+s)(a_2^2+s)(a_3^2+s)}}ds, \tag{A8}$$

with

$$\frac{y_1^2}{a_1^2+\lambda}+\frac{y_2^2}{a_2^2+\lambda}+\frac{y_3^2}{a_3^2+\lambda}=1; \tag{A9}$$

and

$$\phi=\frac{3}{4}\int_{\mu}^{\infty}\frac{1-\left(\frac{z_1^2}{a_1^2+s}+\frac{z_2^2}{a_2^2+s}+\frac{z_3^2}{a_3^2+s}\right)}{\sqrt{(a_1^2+s)(a_2^2+s)(a_3^2+s)}}ds, \tag{A10}$$

with

$$\frac{z_1^2}{a_1^2+\mu}+\frac{z_2^2}{a_2^2+\mu}+\frac{z_3^2}{a_3^2+\mu}=1. \tag{A11}$$

The coordinate transformation for y_i and z_i is defined such that

$$y_1=z_1=x_1,\quad y_2=z_2=x_2,\quad y_3+h=z_3-h=x_3. \tag{A12}$$

It was found that the integrals represented by Eqs. (A8) and (A10), which require the roots of Eqs. (A9) and (A11), respectively, for λ and μ, can be obtained analytically in terms of elementary functions if at least two of the semi-axes a_1, a_2, and a_3 are equal.[30] We make use this property in our analysis of subsurface EI influence on the material band structure.

Effective Poisson's ratio in materials with wurtzite crystal structure

Poisson's ratio ν of a material is defined as $\nu=-\varepsilon_{\text{trans}}/\varepsilon_{\text{long}}$, where $\varepsilon_{\text{long}}$ and $\varepsilon_{\text{trans}}$ are the longitudinal and the transverse strain responses, respectively, to a longitudinal tensile stress (load) σ_{long}. It is assumed that the transverse direction is stress free.

Wurtzite GaN is elastically anisotropic; hence, the Poisson's ratio is also anisotropic. Here, we choose to use an isotropic Poisson ratio $\overline{\nu}$, which is obtained by averaging the three Poisson ratios along the three Cartesian axes, which correspond to high symmetry directions of wurtzite. These individual Poisson's ratios are obtained using the Hooke's law relation between normal stresses and strains in a case of elastic anisotropy:

$$\begin{pmatrix}\varepsilon_{xx}\\ \varepsilon_{yy}\\ \varepsilon_{zz}\end{pmatrix}=\begin{pmatrix}s_{11} & s_{12} & s_{13}\\ s_{12} & s_{11} & s_{13}\\ s_{13} & s_{13} & s_{13}\end{pmatrix}\begin{pmatrix}\sigma_{xx}\\ \sigma_{yy}\\ \sigma_{zz}\end{pmatrix}, \tag{A13}$$

where s_{ij} are the elastic compliance constants in Voigt notation.[48]

In the following, we express the Poisson ratio $\nu_{x(y,z)}$ in terms of the stiffness constants by setting $\sigma_{xx(yy,zz)}=\sigma_{\text{long}}$, and the two remaining stresses to zero as the transverse directions are free surfaces. Since the xy plane is chosen normal to the c direction, it is elastically isotropic. Thus, the transverse strain is also isotropic in this plane for a given longitudinal strain along the z axis. Thus, for $\sigma_{zz}=\sigma_{\text{long}}$, we obtain

$$s_{13}\times\sigma_{\text{long}}=\varepsilon_{xx}=\varepsilon_{yy},\quad s_{33}\times\sigma_{\text{long}}=\varepsilon_{zz}, \tag{A14}$$

leading to

$$\nu_z=-\frac{s_{13}}{s_{33}}. \tag{A15}$$

However, the xz and yz planes are anisotropic. Thus, for $\sigma_{xx(yy)}=\sigma_{\text{long}}$, we get

$$s_{11}\times\sigma_{\text{long}}=\varepsilon_{xx(yy)},\quad s_{12}\times\sigma_{\text{long}}=\varepsilon_{yy(xx)},\quad s_{13}\times\sigma_{\text{long}}=\varepsilon_{zz}. \tag{A16}$$

We define an average Poisson's ratio along x (and y) by

$$\nu_x=\nu_y=-\frac{s_{12}+s_{13}}{2s_{11}}. \tag{A17}$$

Finally, we obtain

$$\overline{\nu}=\frac{2\nu_x+\nu_z}{3}=-\frac{1}{3}\left(\frac{s_{13}}{s_{33}}+\frac{s_{12}+s_{13}}{s_{11}}\right). \tag{A18}$$

[1] G. L. Bir and G. E. Pikus, *Symmetry and Strain Induced Effects in Semiconductors* (Wiley, New York, 1974).
[2] J. Singh, *Electronic and Optoelectronic Properties of Semiconductor Structures* (Cambridge University Press, Cambridge, UK, 2003).
[3] S. Ghosh, P. Waltereit, O. Brandt, H. T. Grahn, and K. H. Ploog, Phys. Rev. B **65**, 075202 (2002).
[4] K. Hoshino, S. Kako, and Y. Arakawa, Phys. Status Solidi B **240**, 322 (2003).
[5] H. K. Cho, J. Y. Lee, J. H. Song, P. M. Yu, S. M. Yang, and C. S. Kim, J. Appl. Phys. **91**, 1104 (2002).
[6] D. Leonard, K. Pond, and P. M. Petroff, Phys. Rev. B **50**, 11687 (1994).
[7] D. Bimberg, M. Grubdmann, and N. N. Ledentsov, MRS Bull. **23**, 31 (1998).
[8] R. J. Warburton, Contemp. Phys. **43**, 351 (2002).
[9] S. Kret, T. Benabbas, C. Delamarre, Y. Androussi, A. Dubon, J. Y. Laval, and A. Lefebvre, J. Appl. Phys. **86**, 1988 (1999).
[10] A. D. Andreev, J. R. Downes, D. A. Faux, and E. P. O'Reilly, J. Appl. Phys. **86**, 297 (1999).
[11] M. Grundmann, O. Stier, and D. Bimberg, Phys. Rev. B **52**, 11969 (1995).
[12] H. Jiang and J. Singh, Physica E (Amsterdam) **2**, 614 (1998).
[13] N. Usami, T. Ichitsubo, T. Ujihara, T. Takahashi, K. Fujiwara, G. Sazaki, and K. Nakajima, J. Appl. Phys. **94**, 916 (2003).
[14] J. H. Davies, J. Appl. Phys. **84**, 1358 (1998).
[15] K. Kash, J. M. Worlock, M. D. Sturge, P. Grabbe, J. P. Harbison, A. Scherer, and P. S. D. Lin, Appl. Phys. Lett. **53**, 782 (1988).
[16] K. Kash, R. Bhat, D. D. Mahoney, P. S. D. Lin, A. Scherer, J. M. Worlock,

B. P. Van der Gaag, M. Koza, and P. Grabbe, Appl. Phys. Lett. **55**, 681 (1989).
[17]G. W. Bryant, J. Lumin. **70**, 108 (1996).
[18]J. Tulkki and A. Heinämäki, Phys. Rev. B **52**, 8239 (1995).
[19]H. Lipsanen, M. Sopanen, and J. Ahopelto, Phys. Rev. B **51**, 13868 (1995).
[20]J. H. Davies, Appl. Phys. Lett. **75**, 4142 (1999).
[21]W. V. Schoenfeldt, C. Metzner, E. Letts, and P. M. Petroff, Phys. Rev. B **63**, 205319 (2001).
[22]J. H. Davies, D. E. Petticrew, and A. R. Long, Phys. Rev. B **58**, 10789 (1998).
[23]A. D. Andreev and E. P. O'Reilly, Phys. Rev. B **62**, 15851 (2000).
[24]P. Waltereit, A. E. Romanov, and J. S. Speck, Appl. Phys. Lett. **81**, 4754 (2002).
[25]G. S. Pearson and D. A. Faux, J. Appl. Phys. **88**, 730 (2000).
[26]E. Pan and B. Yang, J. Appl. Phys. **90**, 1487 (2001).
[27]Q. X. Pei, C. Lu, and Y. Y. Wang, J. Appl. Phys. **93**, 1487 (2003).
[28]M. A. Makeev and A. Madhukar, Phys. Rev. B **67**, 073201 (2003).
[29]E. Pan and B. Yang, J. Appl. Phys. **93**, 2435 (2003).
[30]A. E. Romanov, G. E. Beltz, W. T. Fisher, P. M. Petroff, and J. S. Speck, J. Appl. Phys. **89**, 4523 (2001).
[31]J. D. Eshelby, Proc. R. Soc. London, Ser. A **241**, 376 (1957).
[32]J. D. Eshelby, Proc. R. Soc. London, Ser. A **252**, 561 (1959).
[33]T. Benabbas, Y. Androussi, and A. Levebre, J. Appl. Phys. **86**, 1945 (1999).
[34]G. Maralidharan, Jpn. J. Appl. Phys., Part 2 **39**, L658 (2000).
[35]X. Su, R. K. Kalia, A. Nakano, and P. Vashista, Appl. Phys. Lett. **79**, 4577 (2001).
[36]M. A. Makeev and A. Madhukar, Appl. Phys. Lett. **81**, 3789 (2002).
[37]T. Mura, *Micromechanics of Defects in Solids* (Martinus Nijhoff, Boston, 1987).
[38]M. Tchounkeu, O. Briot, B. Gil, J. P. Alexis, and R.-L. Aulombard, J. Appl. Phys. **80**, 5352 (1996).
[39]Z. X. Liu, S. Pau, K. Syassen, J. Kuhl, W. Kim, H. Morkoç, M. A. Khan, and C. J. Sun, Phys. Rev. B **58**, 6696 (1998).
[40]S. L. Chuang and C. S. Chang, Phys. Rev. B **54**, 2491 (1996).
[41]G. B. Ren, Y. M. Liu, and P. Blood, J. Appl. Phys. **74**, 1117 (1999).
[42]R. Langer, J. Simon, V. Oritz, N. T. Pelekanos, A. Barski, R. Andre, and M. Godlewski, Appl. Phys. Lett. **74**, 3827 (1999).
[43]P. Lefebvre, J. Allegre, B. Gil, H. Mathieu, N. Grandjean, M. Leroux, J. Massies, and P. Bigenwald, Phys. Rev. B **59**, 15363 (1999).
[44]R. Cingolani, A. Botchkarev, H. Tang, H. Morkoc, G. Traetta, G. Coli, M. Lomascolo, A. Di Carlo, F. Della Sala, and P. Lugli, Phys. Rev. B **61**, 2711 (2000).
[45]A. Thamm, O. Brandt, J. Ringling, A. Trampert, K. H. Ploog, O. Mayrock, H.-J. Wunsche, and F. Henneberger, Phys. Rev. B **61**, 16025 (2000).
[46]M. E. Lines and A. M. Glass, *Principles and Applications of Ferroelectrics and Related Materials* (Clarendon, Oxford, 1977).
[47]W. Ludwig, *Festkorperphysik* (Akademische Verlagsgesellschaft, Wiesbaden, 1978).
[48]J. F. Nye, *Physical Properties of Crystals* (Oxford University Press, Oxford, 1957).
[49]P. Waltereit, O. Brandt, A. Trampert, H. T. Grahn, J. Menniger, M. Ramsteiner, M. Reiche, and K. H. Ploog, Nature (London) **406**, 865 (2000).
[50]J. Brown, F. Wu, P. M. Petroff, and J. S. Speck, Appl. Phys. Lett. **84**, 690 (2004.
[51]K. Kim, W. R. L. Lambrecht, and B. Segall, Phys. Rev. B 56, 7018 (1997).
[52]I. Vurgaftman and J. R. MEyer, J. Appl. Phys. **94**, 3675 (2003).
[53]C. Van de Walle (private communication).
[54]F. Bernardini, V. Fiorentini, and D. Vanderbilt, Phys. Rev. B **56**, R10024 (1997).
[55]O. Ambacher, M. Eickhoff, A. Link, M. Hermann, M. StutZmann, F. Bernardini, V. Fiorentini, Y. Smorchkova, J. Speck, U. Mishra, W. Schaff, V. Tilak, and L. F. Eastman, Phys. Status Solidi C **0**, 1878 (2003).
[56]M. D. McCluskey, C. G. Van de Walle, L. T. Romano, B. S. Krusor, and N. M. Johnson, J. Appl. Phys. **93**, 4340 (2003).
[57]See, e.g., the freeware program 1D Poisson/Schrodinger by G. Snider: http://www.nd.edu/~gsnider/
[58]K. Seo and T. Mura, J. Appl. Mech. **46**, 568 (1979).
[59]O. Brandt, P. Waltereit, and K. H. Ploog, J. Phys. D **35**, 577 (2002).